Si dielectric function in a local basis representation: Optical properties, local field effects, excitons, and stopping power

M. Gómez,[1,*] P. González,[1,†] J. Ortega,[2,‡] and F. Flores[2,§]
[1]*Departamento de Física Aplicada, Universidad de Salamanca. 37003-Salamanca, Spain*
[2]*Departamento de Física Teórica de la Materia Condensada, Universidad Autónoma and Condensed Matter Physics Center (IFIMAC), 28049-Madrid, Spain*
(Received 3 July 2014; published 17 November 2014)

An atomiclike basis representation is used to analyze the dielectric function $\epsilon(\vec{q}+\vec{G},\vec{q}+\vec{G}';\omega)$ of Si. First, we show that a sp^3d^5 local basis set yields good results for the electronic band structure of this crystal and, then, we analyze the Si optical properties including local field and excitonic effects. In our formulation, we follow Hanke and Sham [W. Hanke and L. J. Sham, Phys. Rev. B **12**, 4501 (1975); **21**, 4656 (1980)], and introduce excitonic effects using a many-body formulation that incorporates a static screened electron-hole interaction. Dynamical effects in this interaction are also analyzed and shown to introduce non-negligible corrections in the optical spectrum. Our results are found in reasonable agreement with the experimental evidence and with other theoretical results calculated with the computationally more demanding plane-wave representation. Finally, calculations for the stopping power of Si are also presented.

DOI: 10.1103/PhysRevB.90.205210 PACS number(s): 71.15.Ap, 71.10.−w, 71.35.Cc, 78.70.−g

I. INTRODUCTION

The ground-state electronic properties of a crystal are described generally by its electronic bands, whose k-space structure and density of states can be measured with direct or inverse photoemission spectroscopy [1]. Other properties, like their optical excitations or their stopping power, depend on electronic interband transitions that are more conveniently analyzed by the dielectric function $\epsilon(\vec{r},\vec{r}';\omega)$ or its Fourier transform $\epsilon(\vec{q}+\vec{G},\vec{q}+\vec{G}';\omega)$ [1] which, appropriately used, introduces local field effects.

Many groups have analyzed that dielectric function using a plane-wave representation, introducing many-body effects, necessary to include exciton effects associated with the attraction between the excited electron and its hole, by means of either a TDDFT (time-dependent density functional theory) or a Bethe-Salpeter approach [1–4]. Other groups have used a local orbital basis representation [5,6] or a reduced linear combination of those orbitals [7] to calculate $\epsilon(\vec{q}+\vec{G},\vec{q}+\vec{G}';\omega)$ for clusters [5,6] or solids [7]. Although this local orbital approach is more suitable for describing systems with a broken symmetry (surfaces or clusters), we have also found it convenient to reanalyze also how the local orbital basis representation works in crystals such as Si, introducing many-body effects in the way explained by Hanke and Sham [8,9]. Apparently, the main limitation of this approach is related to the very large dimension of the matrices one has to invert: this dimension is $n\alpha^2\rho$, n being the number of atoms in the primitive cell, α the number of orbitals per atom used in the basis set, and ρ the number of interacting neighbors introduced in the calculation, the dimension of these matrices can be as large as 5000 for the most accurate calculation performed in this work. However, in spite of the large dimension of the matrices we have to manage in our approach, the calculations performed to obtain the excitonic properties are not as time consuming as the ones needed in the plane-wave representation [1], allowing us to go a step further including dynamical effects in the screened electron-hole interaction.

In this paper, we start from the conventional formalism [8–10] for the dielectric function and describe how to calculate $\epsilon(\vec{q}+\vec{G},\vec{q}+\vec{G}';\omega)$ using a local orbital representation. Then, we calculate the electronic bands for Si using a local orbital DFT approach [11] with different basis sets of numerical atomiclike orbitals (sp^3, $sp^3s^*p^{*3}$, or sp^3d^5), and analyze the quality of the different basis sets using the f-sum rule for $\epsilon(\vec{q}+\vec{G},\vec{q}+\vec{G}';\omega)$. We conclude that the optimized sp^3d^5 basis set provides a good approximation for calculating $\epsilon(\vec{q}+\vec{G},\vec{q}+\vec{G}';\omega)$. Next, we analyze the Si optical properties including local field and exciton effects [8,9] and show that our sp^3d^5 basis set yields a good description of those optical properties; in the exciton case, we also discuss how dynamical effects can modify the conventionally static approximation for the electron-hole interaction of the exciton [1,8,9]. Finally, we analyze the Si stopping power introducing only local field effects since exciton effects are not expected to be important in this case. In the final section, we present our conclusions and argue that the sp^3d^5 basis set yields an appropriate description of the Si optical properties including exciton effects and, probably, a very convenient way of analyzing complex structures such as clusters and surfaces.

II. DIELECTRIC FUNCTION AND f-SUM RULES

A. Dielectric function

Based on very general arguments, we can write the following equation for the electronic dielectric response [10]:

$$\epsilon^{-1}(\vec{r},\vec{r}';\omega)=\delta(\vec{r}-\vec{r}')+\int\frac{4\pi e^2}{|\vec{r}-\vec{r}''|}\chi(\vec{r}'',\vec{r}',\omega)d^3r'' \quad (1)$$

with the electron polarizability $\chi(\vec{r}'',\vec{r}',\omega)$, defined by the following equation:

$$\rho^{ind}(\vec{r};\omega)=+\int e^2\chi(\vec{r},\vec{r}',\omega)V^{ext}(\vec{r}',\omega)d^3r', \quad (2)$$

*maximo@usal.es
†pgecp@usal.es
‡jose.ortega@uam.es
§fernando.flores@uam.es

where $\rho^{ind}(\vec{r};\omega)$ is the induced electron charge and $V^{ext}(\vec{r}',\omega)$ the external potential. In random phase approximation (RPA), Eq. (1) is replaced by

$$\rho^{ind}(\vec{r};\omega) = + \int e^2 \chi_0(\vec{r},\vec{r}',\omega) V^t(\vec{r}',\omega) d^3r', \tag{3}$$

$\chi_0(\vec{r},\vec{r}',\omega)$ being the free-electron polarizability of the system and $V^t(\vec{r}',\omega) = V^{ext} + V^{ind}$, V^{ind} being defined by

$$V^{ind}(\vec{r},\omega) = \int \frac{4\pi}{|\vec{r}-\vec{r}'|} \rho^{ind}(\vec{r}';\omega) d^3r'. \tag{4}$$

Then, the RPA approximation for $\epsilon(\vec{r},\vec{r}';\omega)$ reads as follows:

$$\epsilon_{\rm RPA}(\vec{r},\vec{r}';\omega) = \delta(\vec{r}-\vec{r}') - \int \frac{4\pi e^2}{|\vec{r}-\vec{r}''|} \chi_0(\vec{r}'',\vec{r}',\omega) d^3r''. \tag{5}$$

For a crystal, it is convenient to write Eq. (5) Fourier transforming the coordinates $(\vec{r},\vec{r}')$ to $(\vec{q}+\vec{G},\vec{q}+\vec{G}')$, where $\vec{G}$ and $\vec{G}'$ are reciprocal lattice wave vectors, $\vec{q}$ belonging to the first Brillouin Zone; this yields [8,12]

$$\begin{aligned}\epsilon_{\rm RPA}(\vec{q}+\vec{G},\vec{q}+\vec{G}';\omega) \\ = \delta_{\vec{G}\vec{G}'} - v(\vec{q}+\vec{G}) \chi_0(\vec{q}+\vec{G},\vec{q}+\vec{G}',\omega),\end{aligned} \tag{6}$$

where $v(\vec{q}+\vec{G}) = 4\pi e^2/\Omega_0 |\vec{q}+\vec{G}|^2$ (Ω_0 being the unit-cell volume). In Eq. (6), $\chi_0(\vec{q}+\vec{G},\vec{q}+\vec{G}',\omega)$ can be calculated from the electron band structure of the crystal, as defined by the electron energy bands $E_n(\vec{k})$ and the corresponding wave functions: $|\Phi^n(\vec{k})\rangle = \sum_{\alpha,i} C^n_{\alpha,i}(\vec{k}) |\alpha,\vec{R}_i\rangle$; here, $|\alpha,\vec{R}_i\rangle$ defines the local orbital basis set used in our calculations (see following). This procedure yields

$$\chi_0(\vec{q}+\vec{G},\vec{q}+\vec{G}',\omega) = \sum_{s,s'} A_s(\vec{q}+\vec{G}) N^0_{ss'}(\vec{q},\omega) A^*_{s'}(\vec{q}+\vec{G}') \tag{7}$$

with

$$\begin{aligned}A_s(\vec{q}+\vec{G}) &= A_{\alpha_i\beta_j\rho_{ij}}(\vec{q}+\vec{G}) \\ &= \exp[-i\vec{G}\cdot\vec{\tau}_j] \langle \alpha_j,0| \exp[-i(\vec{q}+\vec{G})\cdot\vec{r}] |\beta_i,\vec{\rho}_{ij}\rangle \\ &= \exp[-i\vec{G}\cdot\vec{\tau}_j] \int \phi^*_{\alpha_j}(\vec{r}) \exp[-i(\vec{q}+\vec{G})\cdot\vec{r}] \\ &\quad \times \phi_{\beta_i}(\vec{r}-\vec{\rho}_{ij}) d^3r,\end{aligned} \tag{8}$$

where $\vec{\rho}_{ij} = \vec{\tau}_i - \vec{\tau}_j + \vec{R}$ defines the relative position between the atoms with orbitals $\phi_{\alpha i}$ and $\phi_{\beta i}$, and

$$\begin{aligned}N^0_{ss'}(\vec{q},\omega) &= N^0_{(\alpha_i\beta_j\rho_{ij})(\gamma_k\delta_k\rho_{kl})} \\ &= \sum_{n1,n2} \sum_{\vec{k}} \exp[-i(\vec{k}+\vec{q})\cdot\vec{\rho}_{ij}] \exp[+i(\vec{k}+\vec{q})\cdot\vec{\rho}_{kl}] \\ &\quad \times C^{n_2*}_{\beta_j}(\vec{k}) C^{n_1}_{\alpha_i}(\vec{k}+\vec{q}) C^{n_1*}_{\delta_l}(\vec{k}+\vec{q}) C^{n_2}_{\gamma_k}(\vec{k}) \\ &\quad \times \frac{2}{N} \frac{f_{n1}(\vec{k}+\vec{q}) - f_{n2}(\vec{k})}{E_{n_1}(\vec{k}+\vec{q}) - E_{n_2}(\vec{k}) - \omega - i\eta}.\end{aligned} \tag{9}$$

In these equations, $f(\vec{k})$ is the Fermi distribution function and N the number of primitive cells in the crystal. The inverse of this dielectric function [Eq. (6); as a matrix of components $\vec{G}$ and $\vec{G}'$] defines $\epsilon^{-1}_{\rm RPA}(\vec{q}+\vec{G},\vec{q}+\vec{G}';\omega)$, which will be used in Sec. V to calculate the stopping power of a moving charge in Si; this quantity can be readily calculated using a $(\vec{G},\vec{G}')$ matrix (typically of 100th or 200th order), or inverting the matrices $N^0_{ss'}$ with $s \times s$ elements, where $s = 2\alpha^2\rho$ as defined by the number of local orbitals per atom α used in our basis set (see following), and the number of neighbors ρ introduced in the calculation. Then, proceeding in this way, $\epsilon^{-1}_{\rm RPA}(\vec{q}+\vec{G},\vec{q}+\vec{G}';\omega)$ can be written as follows:

$$\begin{aligned}&\epsilon^{-1}_{\rm RPA}(\vec{q}+\vec{G},\vec{q}+\vec{G}';\omega) \\ &\quad = \delta_{\vec{G}\vec{G}'} + v(\vec{q}+\vec{G}) \sum_{s,s'} A_s(\vec{q}+\vec{G}) S_{ss'}(\vec{q},\omega) A^*_{s'}(\vec{q}+\vec{G}'),\end{aligned} \tag{10}$$

where the matrix N^0 in Eq. (7) has been replaced by S:

$$S = N^0[I - VN^0]^{-1} \tag{11}$$

with

$$\begin{aligned}V_{ss'}(\vec{q}) = \frac{1}{\Omega_0} \sum_{\vec{R}_0} \exp[-i\vec{q}\cdot(\vec{\tau}_j - \vec{\tau}_k + \vec{R}_0)] \int d^3r \int d^3r' \\ \times \phi^*_{\alpha_i}(\vec{r}-\vec{\tau}_i-\vec{R}-\vec{R}_0) \phi_{\beta_j}(\vec{r}-\vec{\tau}_j-\vec{R}_0) \frac{e^2}{|\vec{r}-\vec{r}'|} \\ \times \phi^*_{\gamma_k}(\vec{r}'-\vec{\tau}_k) \phi_{\delta_l}(\vec{r}'-\vec{\tau}_l-\vec{R}').\end{aligned} \tag{12}$$

Calculating $\epsilon^{-1}_{\rm RPA}(\vec{q}+\vec{G},\vec{q}+\vec{G}';\omega)$ through the matrix $S_{ss'}$, instead of inverting the $(\vec{G},\vec{G}')$ matrix, might appear to be not practical because that matrix (as well as $N^0_{ss'}$ and $V_{ss'}$) is too large. However, we have found it convenient to use this approach for introducing excitonic effects, as shown by Hanke and Sham [8,12]: this is important for analyzing the optical properties of semiconductors where those effects are important. The crucial idea is to replace, in Eq. (11), $S = N^0[I - VN^0]^{-1}$ by the matrix $N^0[I - \{V - (1/2)V^X\}N^0]^{-1}$, where V^X is the following exchange potential:

$$\begin{aligned}V^X_{ss'}(\vec{q}) = \frac{1}{\Omega_0} \sum_{\vec{R}_0} \exp[-i\vec{q}\cdot(\vec{\tau}_j - \vec{\tau}_k + \vec{R}_0)] \int d^3r \int d^3r' \\ \times \phi^*_{\alpha_i}(\vec{r}-\vec{\tau}_i-\vec{R}-\vec{R}_0) \phi_{\beta_j}(\vec{r}'-\vec{\tau}_j-\vec{R}_0) \frac{e^2}{|\vec{r}-\vec{r}'|} \\ \times \phi^*_{\gamma_k}(\vec{r}-\vec{\tau}_k) \phi_{\delta_l}(\vec{r}'-\vec{\tau}_l-\vec{R}').\end{aligned} \tag{13}$$

This exchange contribution V_X appears when, in addition to the bubblelike RPA diagrams shown in Fig. 1, other "ladder" diagrams, as the ones shown in Fig. 1, are included; these "ladder" diagrams describe the exciton electron-hole pair interaction as shown by Hanke and Sham (HS) [8].

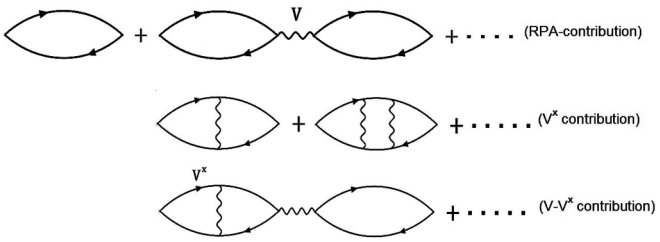

FIG. 1. Diagrams contributing to the HS dielectric function. In the HS approximation, the V^X potential is screened to $V^{X,S}$, using a static dielectric function. Dynamical effects associated with $V^{X,S}$ are discussed in the Appendix.

Then, one can introduce the following Hanke-Sham dielectric function $\epsilon_{\rm HS}^{-1}$:

$$\epsilon_{\rm HS}^{-1}(\vec{q}+\vec{G},\vec{q}+\vec{G}';\omega) = \delta_{\vec{G},\vec{G}'} + v(\vec{q}+\vec{G})\sum_{s,s'} A_s(\vec{q}+\vec{G}) \times N^0[I-\{V-(1/2)V^X\}N^0]^{-1}_{ss'} A_{s'}(\vec{q}+\vec{G}')^*, \quad (14)$$

where the matrix elements $N^0[I-\{V-(1/2)V^X\}N^0]^{-1}_{ss'}$ depend only on the variables $(\vec{q},\omega)$, not on $\vec{G}$ or $\vec{G}'$. Equation (14) will be used in Sec. IV to calculate the optical properties of Si.

We should also mention that this approximation can still be improved by introducing the electron-hole static screened potential $V^{X,S}_{ss'}(q)$, which is obtained by replacing in Eq. (13) $1/|\vec{r}-\vec{r}'|$ by the screened potential $v(\vec{r},\vec{r}') = \int(1/|\vec{r}-\vec{r}''|)\epsilon^{-1}(\vec{r}'',\vec{r}')d^3r''$; in this equation, for the sake of simplicity, $\epsilon(q')$ [the Fourier transform of $\epsilon(\vec{r}''-\vec{r}')$] has been approximated by the Penn dielectric function [13] for $\omega=0$:

$$\epsilon(q) = 1 + \frac{\omega_p^2}{E_g^2+\beta^2q^2+q^4/4} \quad \text{(in a.u.)}, \quad (15)$$

where ω_p is the plasmon frequency (18 eV $\cong$ 0.66 a.u.), E_g the mean optical gap (4.1 eV $\cong$ 0.15 a.u.), and $\beta =$ 0.022 a.u. Therefore, we will take [8,9] in the HS dielectric function $N^0[I-\{V-(1/2)V^{x,s}\}N^0]^{-1}_{ss'}$ instead of $N^0[I-\{V-(1/2)V^X\}N^0]^{-1}_{ss'}$.

In the Appendix, we analyze how to introduce approximately a dynamical screening of V^X; our discussion shows that these dynamical processes can be approximately incorporated in the previous approach [Eq. (14)] by reducing the static screening by a factor of 0.87, namely, taking $(0.435)V^{x,s}$ instead of $(0.5)V^{x,s}$. Results introducing this approximation are also discussed in the following.

B. f-sum rules

We mention now that the following f-sum rule should be satisfied by all the dielectric functions if the basis set used in the calculations is complete [14]:

$$\int_0^\infty \omega\,\mathrm{Im}[\epsilon(\vec{q},\vec{q};\omega)]d\omega = \frac{\pi}{2}\omega_p^2; \quad (16)$$

here, $\omega_p^2 = 4\pi n(q)e^2/m$ $(n=N/\Omega_0)$ defines the plasmon frequency, N being the number of electrons in the primitive cell. It is also convenient to introduce $N(\vec{q},\vec{G},\vec{G}')$ defined as

$$N(\vec{q},\vec{G},\vec{G}') = \frac{m\Omega_0}{2\pi^2e^2}\int_0^\infty \omega\,\mathrm{Im}[\epsilon(\vec{q}+\vec{G},\vec{q}+\vec{G}';\omega)]d\omega \quad (17)$$

such that $N(\vec{q},0,0) = N$ for any $\vec{q}$, if the calculation of the dielectric function is sufficiently accurate. Equation (17), with $\epsilon=\epsilon_{\rm RPA}$, will be used in the following to check the accuracy of the different basis sets used in our calculations

III. LOCAL ORBITAL BASIS: BANDS AND THE f-SUM RULE

In our calculations, we have used for Si the following basis sets of numerical atomiclike orbitals (NAOs) [15]: (i) Si sp^3 NAOs calculated with the following cutoff radii [15] for the s and p orbitals: $r_{cs}=r_{cp}=5.5$ a.u.; (ii) Si sp^3d^5 NAOs with $r_{cs}=4.8$ a.u., $r_{cp}=5.2$ a.u., $r_{cd}=5.4$ a.u. (for the s-, p-, and d-like orbitals); (iii) double basis set orbitals $sp^3s^*p^{*3}$ with $r_{cs}=r_{cp}=r^{cs*}=r^{cp*}=5.5$ a.u. In the calculations presented in Secs. IV and V, we have used 256 k points in the first Brillouin zone [16].

The core electrons are taken into account by means of norm-conserving pseudopotentials [17]. Figure 2 shows the energy band structure calculated with these different basis sets using the local density approximation (LDA) exchange-correlation potential [18]: the calculations using the sp^3 or $sp^3s^*p^{*3}$ basis sets yield an energy gap which is too large, around 2.5 and 2.1 eV, respectively, compared with the plane-wave LDA result 0.7 eV [19] (the experimental energy gap is 1.1 eV); in general, the electronic band structure for these basis sets is significantly different from the one calculated using a converged plane-wave representation which does not include many-body corrections [19]. The sp^3d^5 basis set yields a much better band structure; we find that our sp^3d^5 local basis set yields very accurate valence bands, and conduction bands that are located around 0.25–0.30 eV higher in energy as compared with the LDA plane-wave results. For example, our energy gap of 1.0 eV should be compared with 0.7 eV for the plane-wave calculations, and our X-point energy gap of 3.85 eV should be compared with 3.57 eV for the second case. Notice that all these LDA calculations do not include many-body corrections.

An independent comparison between the quality of the different basis sets can be performed using the f-sum rule [Eq. (17)]; this sum rule yields an indication of the quality of the basis set from the point of view of the conduction band contribution to the dielectric function. Figure 3 shows $N(\vec{q}) = N(\vec{q},0,0)$ as calculated for the different basis sets using the RPA approximation [Eq. (6)]. From these figures we see that $N(q)$ is closer to 8 (the number of electrons per unit cell) along all the q directions considered, for the sp^3d^5 basis set: in particular, in the limit $q\to 0$, $N(q)$ goes to 7.832, this number showing clearly the good quality of this basis set. In these calculations we have taken ρ, the number of neighbors associated with $s=2\alpha^2\rho$, equal to 29, so that for the sp^3d^5 basis set $s=4698$; this corresponds to going to third neighbors. We have checked that this truncation provides a good approximation to the dielectric function, by calculating $N(q\to 0)$ for a larger number of neighbors; in particular, in

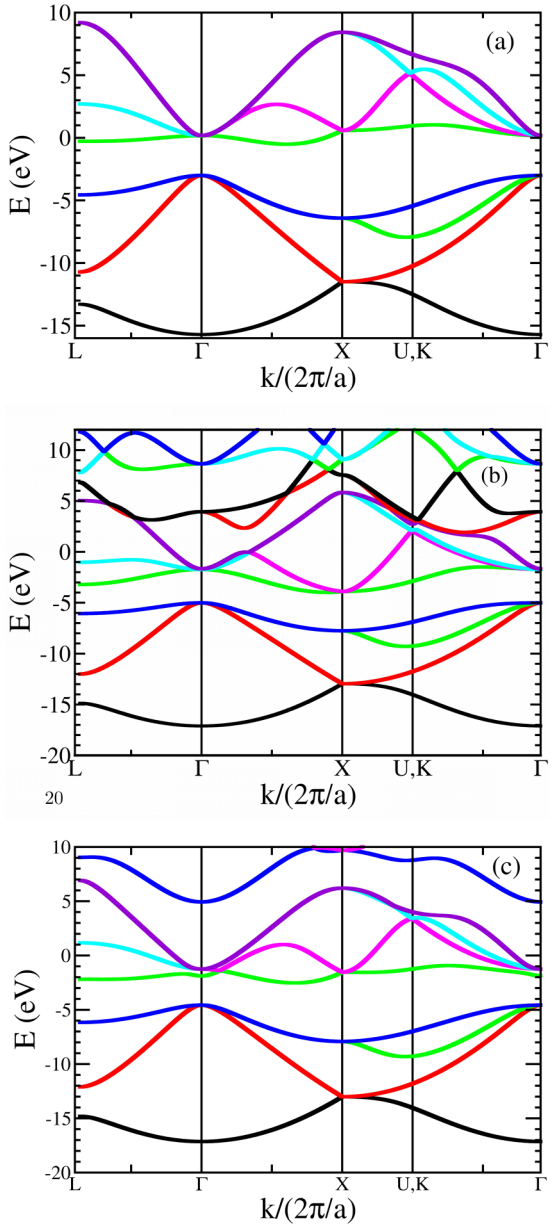

FIG. 2. (Color online) Energy band structure of Si with a basis set of pseudo-orbitals (a) optimized sp^3, (b) sp^3d^5, and (c) $sp^3s^*p^{*3}$.

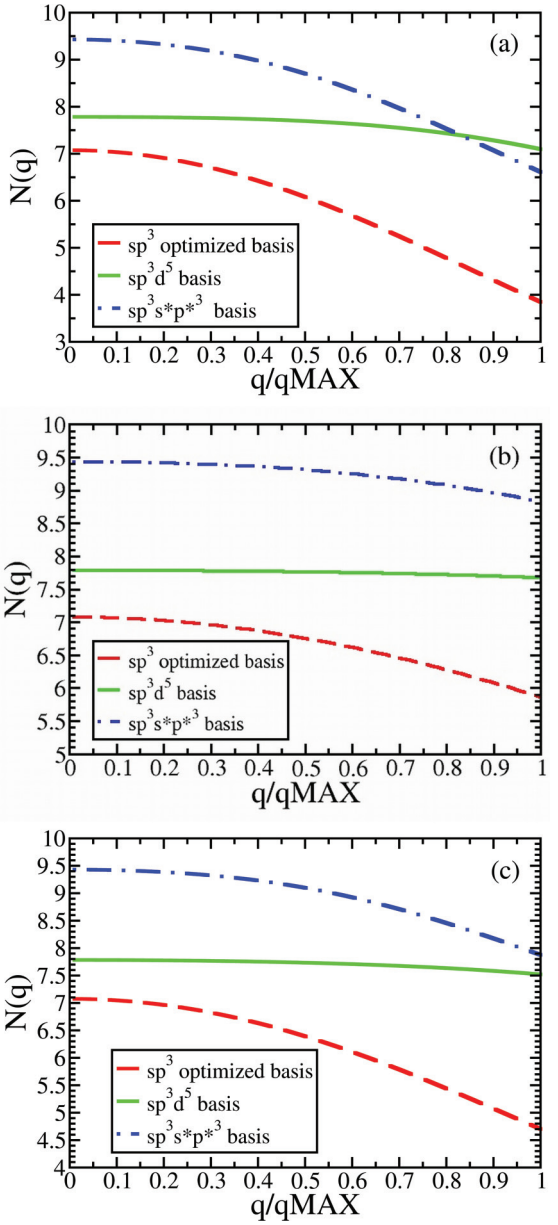

FIG. 3. (Color online) (a) $N(q)$ dependence along the Δ axis of the first Brillouin zone for the optimized sp^3 (broken red line), sp^3d^5 (full green line), and double $sp^3s^*p^{*3}$ (dotted broken blue line) basis set, respectively; $q_{MAX} = (2\pi/a)$. (b) As (a) for the Λ axis of the first Brillouin zone; $q_{MAX} = (\sqrt{3}/2)(2\pi/a)$. (c) As (a) for the Σ axis of the first Brillouin; $q_{MAX} = (3\sqrt{2}/4)(2\pi/a)$.

the sp^3d^5 basis set we have found that, going to fourth, fifth, and sixth neighbors, yields $N(q \to 0) = 7.830$, 7.832, and 7.832, respectively.

Alternatively, we can also discuss the quality of the basis sets by considering the following sum rule: $\langle i|z^2|i\rangle = \sum_j \langle i|z|j\rangle\langle j|z|i\rangle$ applied to the s or p orbitals: notice that the matrix element $\langle j|z|i\rangle$ appears in the calculation of the dielectric function for $q \to 0$, and that satisfying that sum rule is a good indication of the quality of the dielectric function in that limit $q \to 0$. Compare, as an example, the sp^3d^5 and the sp^3 basis sets: for both cases, $\langle s|z^2|s\rangle = 1.61$ Å^2, $\langle p_x|z^2|p_x\rangle = 1.36$ Å^2, and $\langle p_z|z^2|p_z\rangle = 4.07$ Å^2; on the other hand, $\sum_j \langle s|z|j\rangle\langle j|z|s\rangle = 1.58$ Å^2, $\sum_j \langle p_x|z|j\rangle\langle j|z|p_x\rangle = 1.34$ Å^2, and $\sum_j \langle p_z|z|j\rangle\langle j|z|p_z\rangle = 3.36$ Å^2 for the sp^3d^5 basis set, while for the sp^3, $\sum_j \langle s|z|j\rangle\langle j|z|s\rangle = 1.58$ Å^2, $\langle p_x|z^2|p_x\rangle = 0$ Å^2, and $\sum_j \langle p_z|z|j\rangle\langle j|z|p_z\rangle = 1.58$ Å^2. These numbers, and similar results for the $sp^3s^*p^{*3}$, confirm that the sp^3d^5 basis set is much better than the other two, as found above in the analysis of the electronic band structure.

We conclude from our results for the band structure and the sum rules that the sp^3d^5 basis set appears to be a good one for calculating the Si dielectric properties. From now on, we will use that basis set for analyzing the dielectric function of Si and its excitonic properties; we will also discuss in the following the effects associated with the difference in the conduction

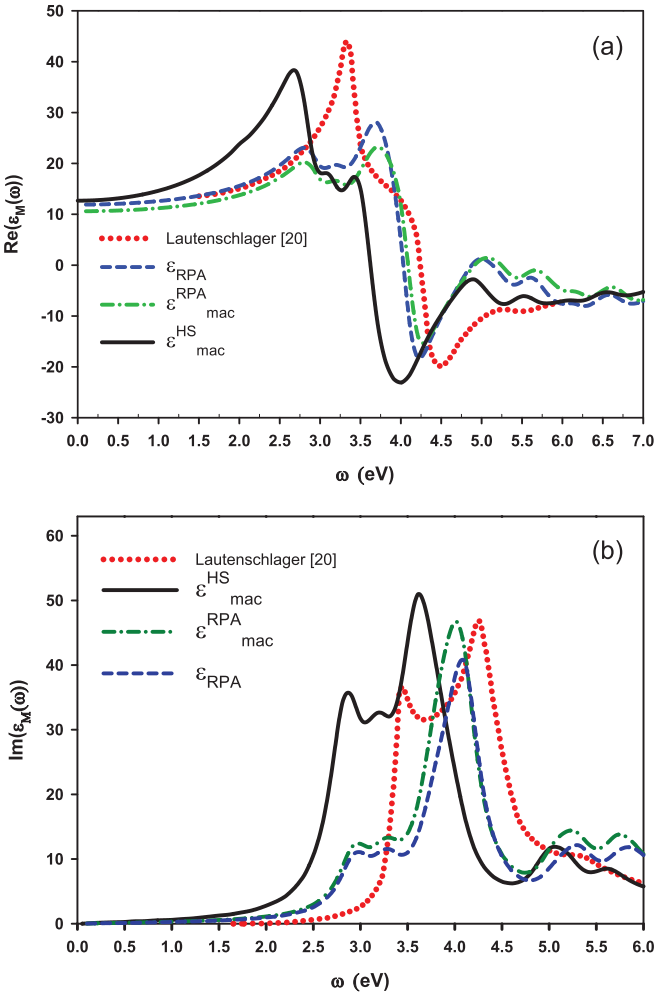

FIG. 4. (Color online) (a) Real and (b) imaginary parts of the dielectric response of Si for the sp^3d^5 basis set and $\vec{q} = (2\pi/a)(0.01,0,0)$. Comparison between the expression (5) $\epsilon_{\rm RPA}(\vec{q},\vec{q};\omega)$ (broken blue line), (18) $\epsilon^{\rm RPA}_{mac}(\vec{q};\omega)$ (dotted broken green line), (19) $\epsilon^{\rm HS}_{mac}(\vec{q};\omega)$ (full black line) and the experimental value (dotted red line) after [20].

band energy levels between using either our local orbital basis or the plane-wave representation.

IV. OPTICAL PROPERTIES

Figure 4 shows Re[$\epsilon_{\rm RPA}(q,\omega)$] and Im[$\epsilon_{\rm RPA}(q,\omega)$] [Eq. (6)] for $\vec{G} = \vec{G}' = 0$ and $\vec{q}$ very small. Although this approach does not include local effects, the long-wavelength limit $q \to 0$, $\epsilon_{\rm RPA}(q,0)$, agrees well with the experimental value of the static dielectric function $\epsilon(q,0) \approx 11$ [21]. The imaginary part of this dielectric function defines the optical absorption in the RPA approximation; this spectrum is, however, far from the experimental data and different steps have to be taken to improve it.

First, local field effects in the optical properties are taken into account by calculating $\epsilon^{-1}_{\rm RPA}(\vec{q}+\vec{G},\vec{q}+\vec{G}';\omega)$ for $\vec{G} = \vec{G}' = 0$ and $q \to 0$, namely, $\epsilon^{-1}_{\rm RPA}(q \to 0;\omega)$, and defining the following macroscopic dielectric function [22,23]:

$$\epsilon^{\rm RPA}_{mac}(\vec{q};\omega) = \frac{1}{\epsilon^{-1}_{\rm RPA}(\vec{q};\omega)}. \tag{18}$$

On the other hand, excitonic effects are introduced by means of the HS dielectric function $\epsilon^{-1}_{\rm HS}(\vec{q}+\vec{G},\vec{q}+\vec{G}';\omega)$. In the same spirit as above, we can also introduce a macroscopic dielectric function, including excitonic effects, as follows [22,23]:

$$\epsilon^{\rm HS}_{mac}(\vec{q};\omega) = \frac{1}{\epsilon^{-1}_{\rm HS}(\vec{q};\omega)}. \tag{19}$$

The real and imaginary parts of $\epsilon^{\rm RPA}_{mac}(\vec{q};\omega)$ and $\epsilon^{\rm HS}_{mac}(\vec{q};\omega)$, $q = (2\pi/a)(0.01,0.0,0.0)$, are shown in Fig. 4 and compared with the results calculated using $\epsilon^{\rm RPA}(\vec{q};\omega)$. Notice that while local field effects introduce a small change in the values of $\epsilon^{\rm RPA}(\vec{q};\omega)$, excitonic effects are more dramatic, introducing an important broadening of the main peak located around 4 eV for Im[$\epsilon^{\rm RPA}(\vec{q};\omega)$].

Figure 4(b) compares our results for Im[$\epsilon^{\rm RPA}(\vec{q};\omega)$], Im[$\epsilon^{\rm RPA}_{mac}(\vec{q};\omega)$], and Im[$\epsilon^{\rm HS}_{mac}(\vec{q};\omega)$] with the experimental optical spectrum for Si. It is interesting to realize that the spectrum calculated with Im[$\epsilon^{\rm HS}_{mac}(\vec{q};\omega)$] is very similar to the experimental one except for a shift of around 0.5 eV to lower energies, indicating that the optical energy gap between our calculated conduction and valence bands $E_c - E_v$ is a little too narrow. This suggests to improve our calculated optical spectrum by introducing in the optical energy gap a correction that can be attributed to the difference between the quasiparticle energies and the energies calculated in LDA [1,12]; following Hybertsen and Louie, we have recalculated our optical spectrum in the HS approximation, using the following correction for $E_c - E_v$:

$$E^{\rm QP}_c - E^{\rm QP}_v = 1.03(E_c - E_v) + 0.69, \tag{20}$$

which practically opens the optical energy gap by 0.7 eV. Figure 5(a) shows Im[$\epsilon^{\rm HS}_{mac}(\vec{q};\omega)$] with this correction, named Im[$\epsilon^{\rm HSQS}_{mac}(\vec{q};\omega)$]; we stress that the new calculated optical spectrum is now in better agreement with the experimental data and close to other theoretical results obtained using a plane-wave representation in combination with the Bethe-Salpeter equation and/or a TDLDA approach [1,24]. One should keep in mind, however, that in our calculations the conduction band is around 0.25 eV too high in energy, suggesting that the correction we have introduced in the conduction band quasiparticle levels is a little too large. We have analyzed this effect in combination with the dynamical effects discussed above by introducing the following corrections: in our final calculations we have taken $0.435V^{x,s}$ instead of $0.5V^{x,s}$ in Eq. (14), and have reduced the quasiparticle correction given by Eq. (20) to

$$E^{\rm QP}_c - E^{\rm QP}_v = 1.03(E_c - E_v) + 0.49. \tag{21}$$

Introducing in this way a shift of 0.2 eV in the conduction bands as suggested by our discussion in Sec. III. Figure 5(b) shows the new results for Im[$\epsilon^{\rm HS}_{mac}(\vec{q};\omega)$], named Im[$\epsilon^{\rm HS*}_{mac}(\vec{q};\omega)$] introducing (a) first the dynamical effects in the electron-hole interaction and (b) also the shift of the

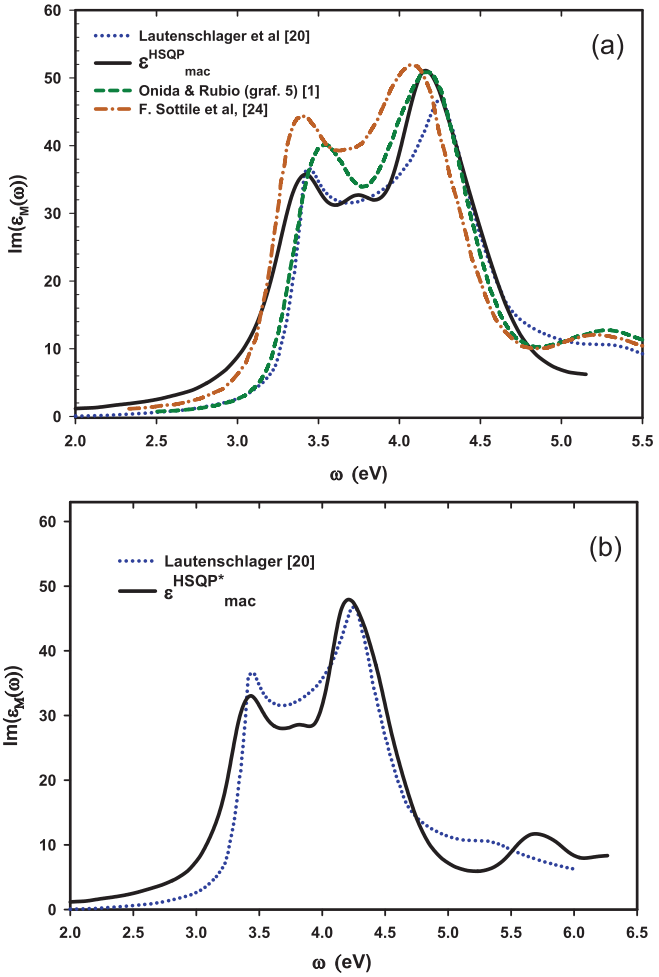

FIG. 5. (Color online) (a) Imaginary part of $\epsilon(\omega)$ in the long-wavelength limit $\vec{G} = \vec{G}' = 0$ for the sp^3d^5 basis set including local and excitonic effects. Dotted blue line: experimental results [20]. Full black line: our results including quasiparticle energy correction ($\epsilon^{\mathrm{HSQP}}_{mac}$). Broken green line: results of Onida and Rubio [1]. Dotted broken brown line: results of Sottile *et al.* [24]. (b) Dotted blue line: experimental results. Full black line: our results including quasiparticle energy correction with dynamic screening, after the Appendix ($\epsilon^{\mathrm{HS}*}_{mac}$).

conduction band. Comparing with the experimental evidence, we find a remarkable agreement between this new spectrum and the experimental data. We stress that if we had not introduced the 0.2-eV shift in the conduction band, the excitonic spectrum would be located 0.2 eV too high in energy. Notice also that the effect of introducing dynamical effects in the screened electron-hole interaction is to shift slightly (around 0.25 eV) the optical spectrum to higher energies, and to change a little the relative weights of the two peaks of the spectrum.

V. STOPPING POWER

The stopping power of a material, in linear theory, for a particle of charge Z, moving with velocity $\vec{v}$ and located at $\vec{R}_I$, is given by [13,25]

$$S(\vec{R}_I,\vec{v}) = -\frac{8\pi Z^2}{\Omega_0 v}\sum_{\vec{G},\vec{G}'}\exp[i(\vec{G}-\vec{G}')\cdot\vec{R}_I]\sum_{\vec{q}}\frac{(\vec{q}+\vec{G})\cdot\vec{v}}{|\vec{q}+\vec{G}|^2} \times \mathrm{Im}[\epsilon^{-1}(\vec{q}+\vec{G},\vec{q}+\vec{G}';\omega=(\vec{q}+\vec{G})\cdot\vec{v})]. \quad (22)$$

For a random trajectory, the energy loss by unit of length is given by

$$\left[-\frac{dE}{dx}\right]_{\mathrm{random}} = -\frac{8\pi Z^2}{\Omega_0 v}\sum_{\vec{G}}\sum_{\vec{q}}\frac{(\vec{q}+\vec{G})\cdot\vec{v}}{|\vec{q}+\vec{G}|^2} \times \mathrm{Im}[\epsilon^{-1}(\vec{q}+\vec{G},\vec{q}+\vec{G};\omega=(\vec{q}+\vec{G})\cdot\vec{v})], \quad (23)$$

where only the diagonal part $\vec{G} = \vec{G}' = 0$ contributes to the stopping power. For high velocity $(\vec{q}+\vec{G})\cdot\vec{v}$ is large, and ϵ^{-1} tends to the classical dielectric function $[1-\omega_p^2/\omega^2]^{-1}$; this yields the Bethe's limit [13,26]

$$\left[-\frac{dE}{dx}\right]_{\mathrm{random}} \approx \frac{4\pi Z^2 e^4}{mv^2} n_0 \ln\left(\frac{2mv^2}{\hbar\omega_p}\right). \quad (24)$$

Equations (22) and (23) show how the inverse of the dielectric function $\epsilon^{-1}(\vec{q}+\vec{G},\vec{q}+\vec{G}';\omega)$ determines the energy loss and the stopping power for a particle moving in a dielectric medium. We analyze this problem using the RPA approximation discussed above because, in this problem, exciton effects are negligible [this simplifies a lot the calculation of $\epsilon^{-1}(\vec{q}+\vec{G},\vec{q}+\vec{G}';\omega)$ that can be inverted in the $(\vec{G};\vec{G}')$ space avoiding to calculate the inverse of larger matrices like $(1-VN)$]. In this regard, it is important to realize that local effects are important in this problem, implying that in previous equations $[\epsilon^{-1}_{\mathrm{RPA}}(\vec{q}+\vec{G},\vec{q}+\vec{G}';\omega)]$ should be used instead

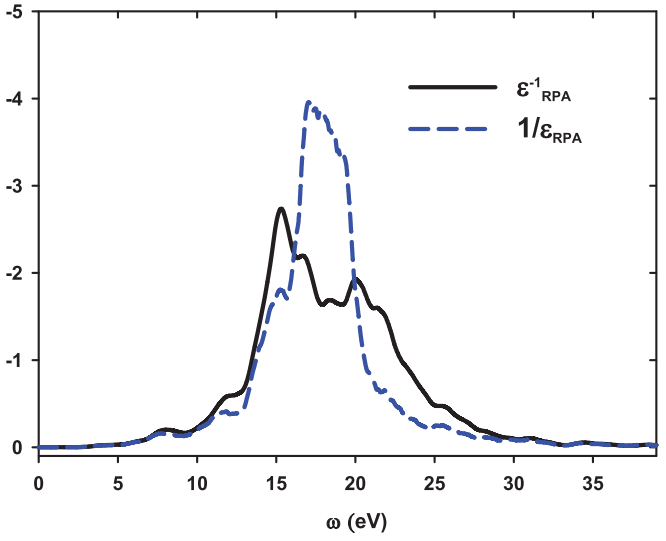

FIG. 6. (Color online) Imaginary part of $\epsilon^{-1}(\vec{q}+\vec{G},\vec{q}+\vec{G}';\omega)$, $q = (0.125,0.125,0.125)(2\pi/a)$, for a sp^3d^5 basis set. Broken blue line: $\mathrm{Im}[1/\epsilon(\vec{q},\vec{q};\omega)]$ obtained from (6), without local effects. Full black line: result according to (5), $\mathrm{Im}[\epsilon^{-1}(\vec{q},\vec{q};\omega)]$, with local effects.

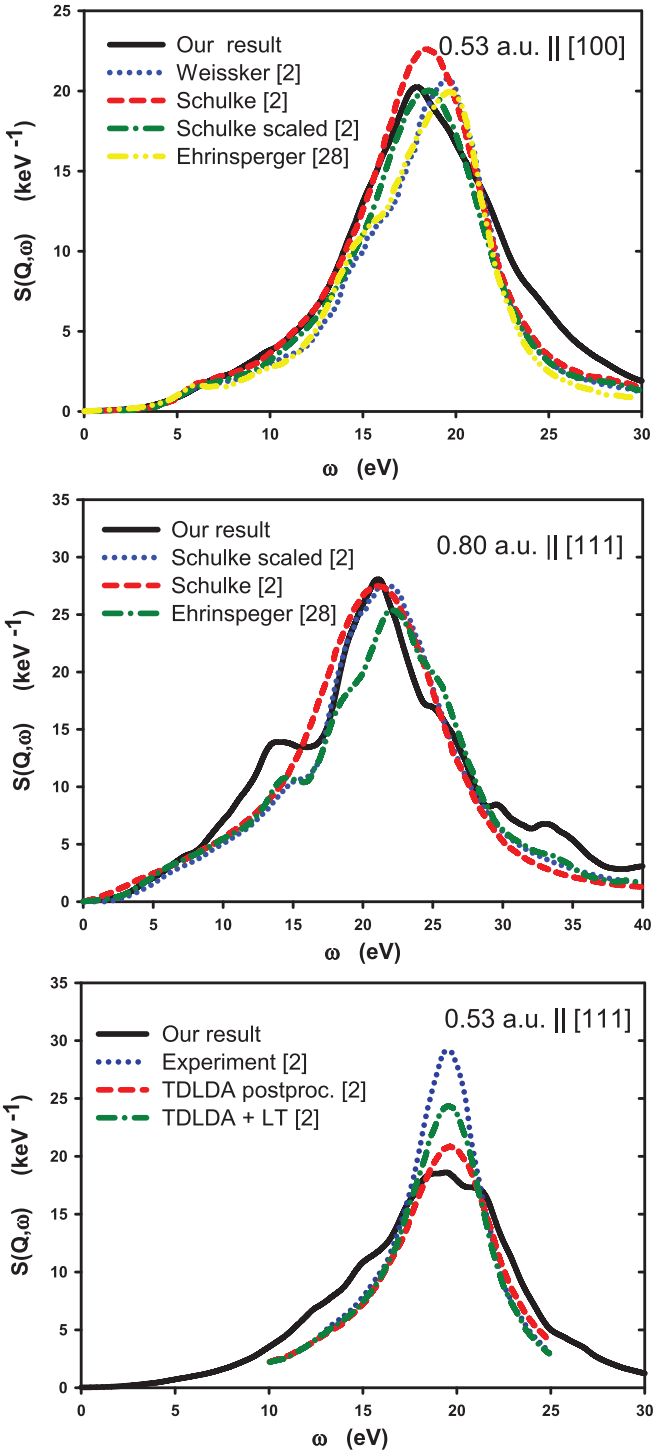

FIG. 7. (Color online) Dynamical structure factor of Si for $\vec{q} = (0.53,0,0)$, $\vec{q} = (0.53,0.53,0.53)$, and $\vec{q} = (0.80,0.80,0.80)$ a.u. Comparison of our results (full black line) with those of [2] and [28].

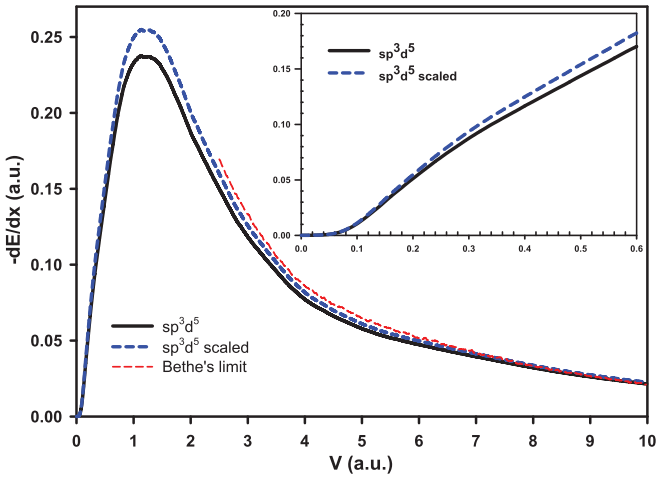

FIG. 8. (Color online) Random stopping power for Si. Full black line: random stopping power as calculated using $\mathrm{Im}[\epsilon^{-1}_{\mathrm{RPA}}]$ for Si [Eq. (10)] for the sp^3d^5 basis set. Broken blue line: results calculated incorporating the correction factor $\alpha(q)$) [Eq. (25)]. Broken red line shows the Bethe limit [see Eq. (24)]. Inset: shows the low-velocity limit. Broken blue line corresponds to incorporating the correction factor $\alpha(q)$.

of $[\epsilon_{\mathrm{RPA}}(\vec{q}+\vec{G},\vec{q}+\vec{G}';\omega)]^{-1}$. This is illustrated in Fig. 6, where we compare our theoretical results for $\mathrm{Im}[\epsilon^{-1}_{\mathrm{RPA}}(\vec{q}+0,\vec{q}+0;\omega)]$ and $\mathrm{Im}[1/\epsilon_{\mathrm{RPA}}(\vec{q}+0,\vec{q}+0;\omega)]$, the first one including local effects introduced by calculating the inverse of the matrix-dielectric function $\epsilon(\vec{q}+\vec{G},\vec{q}+\vec{G}';\omega)$. We can observe from Fig. 6 that local effects broaden the loss function $\mathrm{Im}[\epsilon^{-1}_{\mathrm{RPA}}(\vec{q}+0,\vec{q}+0;\omega)]$ and shift the maximum peak, as obtained by other authors [26,27]. Changes introduced by local effects are important not only for bigger transferred momentums, as Weissker *et al.* [2] have shown, but also for lower ones, as we can deduce from Fig. 6.

In Fig. 7, we compare our calculated structure factor $S(q,\omega) = (q^2/4\pi^2)\mathrm{Im}[\epsilon^{-1}(\vec{q}+0,\vec{q}+0;\omega]$ for different values of q, with the results obtained by different authors using a TDLDA approximation for the dielectric function [1,24]; experimental results [29] are also shown for comparison. In general, we find a good agreement between our results and the other theoretical or experimental data; this suggests that our calculated linear stopping power, as discussed below, can be taken with a high degree of confidence.

Figure 8 shows the linear stopping power of Si including local effects. The sum on reciprocal vectors $\vec{G}$ in Eq. (23) is limited to the condition $|q+G| \leqslant 5(2\pi/a)$. This limit is enough to ensure convergence for the stopping power results at low velocities, where local effects are very important. These calculations have to be corrected, however, because the f-sum rule is not fully fulfilled, as discussed in Sec. III. We have corrected this small discrepancy by introducing a factor $\alpha(\vec{q})$ in $\mathrm{Im}[\epsilon^{-1}_{\mathrm{RPA}}(\vec{q}+\vec{G},\vec{q}+\vec{G};\omega)]$ such that

$$\int_0^\infty \omega \cdot \mathrm{Im}\left[\epsilon^{-1}_{\mathrm{RPA}}(\vec{q},\vec{G},\vec{G};\omega)\right] \cdot \alpha(\vec{q}) d\omega = -\frac{\pi}{2}\omega_p^2, \qquad (25)$$

then, the same factor is introduced in Eq. (23). Figure 8 shows the stopping power as calculated with Eq. (23): the solid line corresponds to using only $\mathrm{Im}[\epsilon^{-1}_{\mathrm{RPA}}(\vec{q}+\vec{G},\vec{q}+\vec{G};\omega)]$, while the dashed line is calculated with $\mathrm{Im}[\alpha(\vec{q})\epsilon^{-1}_{\mathrm{RPA}}(\vec{q}+\vec{G},\vec{q}+\vec{G};\omega)]$. Notice that the correction introduced by $\alpha(\vec{q})$ is rather small, as corresponds to using a basis set that almost fulfills the different sum rules. Moreover, our calculations agree well with the results of other authors [30–32]. At high velocities,

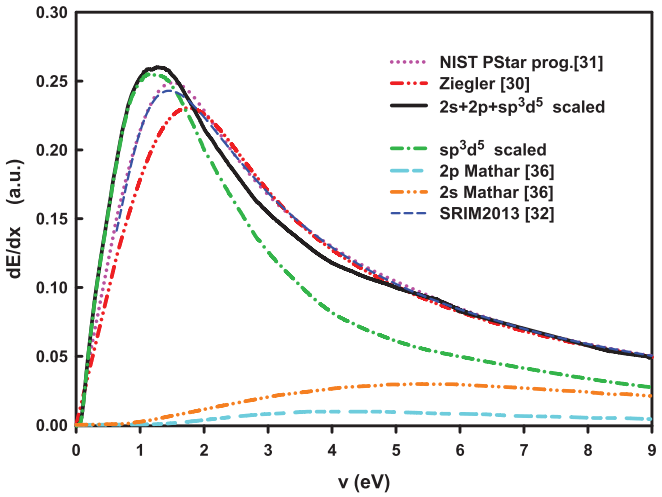

FIG. 9. (Color online) Random stopping power for Si. Doubled dotted broken red line: Ziegler's results for all electrons in Si atom [30]. Dotted red line: NIST PStar program [31] for all electrons in Si atom. Broken blue line: result after SRIM2013 [32] program for all electrons in Si atom. Broken brown line: stopping power of the $2s$ electrons in Si after Mathar [36]. Broken light blue line: stopping power of the $2p$ electrons in Si after Mathar [36]. Dotted broken green line: our result (23) for the sp^3d^5 basis set with the correction due to the factor $\alpha(\vec{q})$ [Eq. (25)]. Full black line: our result (23) for the sp^3d^5 basis set with the correction due to the factor $\alpha(\vec{q})$ [Eq. (25)] plus the $2s$ and $2p$ electrons contributions after Matthar [36].

local effects are not so important and the linear stopping power tends to the Bethe's limit [Eq. (24)]: this can be checked in Fig. 8, where it can be seen how the "corrected" linear stopping power tends to the Bethe´s limit for v larger than 2–3 a.u.

The inset of Fig. 8 also shows enlarged the linear stopping power in the range of low velocities, a range showing a threshold velocity, around 0.1 a.u., associated with the semiconductor energy gap [26,33–35].

Finally, in Fig. 9 we show the total stopping power for a random motion of hydrogen in Si, including the contributions from the Si $2s$ and $2p$ electrons, as calculated by Mathar [36]; in this figure, we also show the experimental data of Ziegler [30,32]. Our calculations agree very well with the experimental data for v larger than 2 a.u.; however, for lower velocities, differences appear that we attribute to nonlinear effects, such as charge exchange processes, nonlinear screening, etc., discussed by other authors [13].

VI. CONCLUSIONS

We have obtained the band structure, the dielectric function, the loss function, and the stopping power for Si in a local pseudo-orbitals basis representation using FIREBALL 2004 code [11]. The sp^3d^5 basis set yields good results and much better than the ones calculated with the sp^3 or the $sp^3s^{*3}p^{*3}$ basis sets; so, the sp^3d^5 local basis can be confidently used for calculating the dynamical dielectric function of Si, if many-body quasiparticle corrections are appropriately introduced.

In particular, we have also shown that by using the Hanke-Sham formulation in this local representation, one can incorporate accurately excitonic effects in the dielectric function, provided quasiparticle corrections are introduced in the energy band levels. This procedure offers an alternative to the plane-wave representation approach developed by other authors for including those excitonic effects in the dielectric function [1,24], the advantage of our approach being that the computational demands needed in the local orbital representation are not as large as those used in the other representation; the basic difference being the matrix, around 5000×5000, we have to invert to calculate the exciton properties, to be compared with a much larger matrix that has to be inverted in the plane-wave representation to calculate the effective electron-hole coupling. This suggests that this local representation approach might be very suitable for analyzing excitons in surfaces, clusters, and noncrystalline solids.

We also mention that we have analyzed the dynamical effects associated with the electron-hole screened potential $V^{x,s}$; our discussion has been based on an analysis of a first-order diagram used to calculate the dielectric function. We have shown that a reasonable description of those dynamical effects can de obtained by replacing the statically screened potential $0.5V^{x,s}$ by $0.435V^{x,s}$. Although these effects are found to be small, they go in the direction of improving the agreement between the theory and the experimental data, provided an appropriate correction of the quasiparticle conduction band levels is introduced.

Finally, we have analyzed the linear stopping power of charged particles in Si, and have shown that, for obtaining accurate results at low and intermediate velocities, local field effects should be included. Our results for the stopping power of hydrogen in Si, after including the contributions from the Si $2s$ and $2p$ shells, agree accurately with the experimental data for velocities v larger than 2–3 a.u.; however, for lower velocities, say v smaller than 1.5 a.u., other effects, such as charge exchange processes and nonlinear screening, should be included [13].

ACKNOWLEDGMENTS

We thank P. García and A. Rubio for interesting discussions. This work has been partially supported by the Spanish Ministerio de Economía y Competitividad (MINECO) under Grants No. TEC 2012-32777 and No. FIS 2010-16046. We also thank E. Velázquez for his assistance with some calculations

APPENDIX: EVALUATION OF THE DYNAMICAL SCREENED POTENTIAL

We have explored the accuracy of having used a static screening for V^x by analyzing the diagram of Fig. 10, where

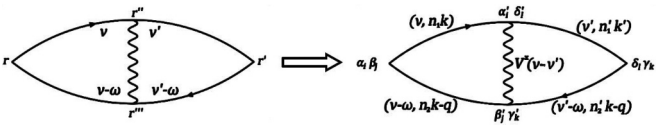

FIG. 10. The first-order diagram proportional to $V^{x,s}(\vec{k}-\vec{k}', v-v')$.

we have used a local representation for describing the different Green's functions; for example, the line joining the points α_i and α_i' represents the following Green's function:

$$G_{\alpha_i,\alpha_i'}(\nu,n_1\vec{k}) = \frac{f_{n_1}(\vec{k})}{\nu - E_{n_1}(\vec{k}) - i0^+} + \frac{1 - f_{n_1}(\vec{k})}{\nu - E_{n_1}(\vec{k}) + i0^+}; \tag{A1}$$

factors like $C^{n_1}_{\alpha_i}(\vec{k})C^{n_1}_{\alpha_i'}(\vec{k})$ are not included for the sake of simplicity. Diagram 10 yields the following contribution:

$$D(\omega) = -\int \frac{d\nu}{2\pi}\int \frac{d\nu'}{2\pi} G_{\alpha_i,\alpha_i'}(\nu)G_{\beta_j,\beta_j'}(\nu-\omega)G_{\delta_l,\delta_l'}(\nu')G_{\gamma_k,\gamma_k'}(\nu'-\omega).V^x_{\alpha'\beta'\delta'\gamma'}\left[\frac{1}{\epsilon^C_{\alpha'\beta'\delta'\gamma'}(\nu-\nu')}\right], \tag{A2}$$

where the causal dielectric function $[1/\epsilon^C_{\alpha'\beta'\delta'\gamma'}(\nu-\nu')] = [1/\epsilon^C_{\alpha'\beta'\delta'\gamma'}(\vec{q}',\nu-\nu')]$, with $\vec{q}' = \vec{k} - \vec{k}'$, is defined as follows:

$$\left[\frac{1}{\epsilon^C_{\alpha'\beta'\delta'\gamma'}(\nu-\nu')}\right] = -\int_0^\infty \frac{d\omega'}{\pi}\frac{\mathrm{Im}[1/\epsilon^C(\omega')]}{\omega'-\nu+\nu'+i0^+} + \int_{-\infty}^0 \frac{d\omega'}{\pi}\frac{\mathrm{Im}[1/\epsilon^C(\omega')]}{\omega'-\nu+\nu'-i0^+}. \tag{A3}$$

If $\epsilon^C(\omega')$ were ω' independent, say $\epsilon^C(0)$, Eq. (A2) would yield

$$D(\omega) = \frac{\{f_{n_1}(\vec{k})[1-f_{n_2}(\vec{k}-\vec{q})] - [1-f_{n_1}(\vec{k})]f_{n_2}(\vec{k}-\vec{q})\}}{\omega - E_{n_1}(\vec{k}-\vec{q}) + E_{n_2}(\vec{k}) + i0^+}\frac{V^x_{\alpha'\beta'\delta'\gamma'}}{\epsilon^C_{\alpha'\beta'\delta'\gamma'}(0)}\frac{\{f_{n_1'}(\vec{k}')[1-f_{n_2'}(\vec{k}'-\vec{q})] - [1-f_{n_1'}(\vec{k}')]f_{n_2'}(\vec{k}'-\vec{q})\}}{\omega - E_{n_1'}(\vec{k}'-\vec{q}) + E_{n_2'}(\vec{k}') - 0^+}, \tag{A4}$$

which represents one of the different terms contributing to Eq. (14) with $V^{x,s} = V^x/\epsilon^C(0)$.

For a general ω dependent $\epsilon^C(\omega)$, we get the following results:

(a) For the term associated with the factor $f_{n_1}(\vec{k})[1-f_{n_2}(\vec{k}-\vec{q})]f_{n_1'}(\vec{k}')[1-f_{n_2'}(\vec{k}'-\vec{q})]$, we find that $[1/\epsilon^C(0)]$ should be replaced by

$$\begin{aligned}[1/\epsilon^C(0)] \to 1 + F_a = 1 &+ \int_0^\infty \frac{d\omega'}{\pi}\frac{\mathrm{Im}[1/\epsilon^C(\omega')]}{[\omega'-\omega-E_{n_2}(\vec{k}-\vec{q})+E_{n_1}(\vec{k})+i0^+]} \\ &- \int_{-\infty}^0 \frac{d\omega'}{\pi}\frac{\mathrm{Im}[1/\epsilon^C(\omega')]}{[\omega'+\omega+E_{n_2'}(\vec{k}-\vec{q})-E_{n_1'}(\vec{k})-i0^+]}.\end{aligned} \tag{A5}$$

Taking $E_{n_2}(\vec{k}-\vec{q}) - E_{n_1}(\vec{k}) \cong E_{n_2'}(\vec{k}-\vec{q}) - E_{n_1'}(\vec{k}) \cong E_g$ (the optical energy gap),

$$1 + F_a = 1 + \int_0^\infty \frac{d\omega'}{\pi}\frac{\mathrm{Im}[1/\epsilon^C(\omega')]}{(\omega'-\omega-E_g+i0^+)} - \int_{-\infty}^0 \frac{d\omega'}{\pi}\frac{\mathrm{Im}[1/\epsilon^C(\omega')]}{(\omega'+\omega+E_g-i0^+)} \tag{A6}$$

or, equivalently,

$$[1/\epsilon^C(0)] \to 1 + F_a = 1 + \int_0^\infty \frac{d\omega'}{\pi}\frac{\mathrm{Im}[1/\epsilon(\omega')]}{(\omega'-\omega-E_g+i0^+)} + \int_{-\infty}^0 \frac{d\omega'}{\pi}\frac{\mathrm{Im}[1/\epsilon(\omega')]}{(\omega'+\omega+E_g+i0^+)}, \tag{A7}$$

where $\epsilon(\omega)$ is the conventional dielectric function $\{\mathrm{Im}[\epsilon(\omega)] = \mathrm{sgn}(\omega)\mathrm{Im}[\epsilon^G(\omega)]\}$.

(b) Similarly, for the term associated with the factor $[1-f_{n_1}(\vec{k})]f_{n_2}(\vec{k}-\vec{q})\cdot[1-f_{n_1'}(\vec{k}')]f_{n_2'}(\vec{k}'-\vec{q})$, we find that $[1/\epsilon^C(0)]$ should be replaced by

$$[1/\epsilon^C(0)] \to 1 + F_b = 1 + \int_0^\infty \frac{d\omega'}{\pi}\frac{\mathrm{Im}[1/\epsilon(\omega')]}{(\omega'+\omega-E_g+i0^+)} + \int_{-\infty}^0 \frac{d\omega'}{\pi}\frac{\mathrm{Im}[1/\epsilon(\omega')]}{(\omega'-\omega+E_g-i0^+)}. \tag{A8}$$

(c) (d) For the other factors $f_{n_1}(\vec{k})[1-f_{n_2}(\vec{k}-\vec{q})]\cdot[1-f_{n_1'}(\vec{k}')]f_{n_2'}(\vec{k}'-\vec{q})$ and $f_{n_1'}(\vec{k}')[1-f_{n_2'}(\vec{k}'-\vec{q})]\cdot[1-f_{n_1}(\vec{k})]f_{n_2}(\vec{k}-\vec{q})$, we find

$$1 + F_c = 1 + F_d = 1 + \int_0^\infty \frac{d\omega'}{\pi}\frac{\mathrm{Im}[1/\epsilon(\omega')]}{(\omega'-E_g+i0^+)} + \int_{-\infty}^0 \frac{d\omega'}{\pi}\frac{\mathrm{Im}[1/\epsilon(\omega')]}{(\omega'+E_g-i0^+)}. \tag{A9}$$

Notice that $F_a(\omega) = F_b(-\omega)$ and $F_a(0) = F_b(0) = F_c = F_d$; this suggests to take

$$F_a \cong F_b \cong F_c = F_d = \int_0^\infty \frac{d\omega'}{\pi}\frac{\mathrm{Im}[1/\epsilon(\omega')]}{(\omega'-E_g+i0^+)} + \int_{-\infty}^0 \frac{d\omega'}{\pi}\frac{\mathrm{Im}[1/\epsilon(\omega')]}{(\omega'+E_g-i0^+)}. \tag{A10}$$

This discussion indicates how to include the dynamical effects associated with $1/\epsilon^{C}(\omega)$ in $V^{x,s}$: by introducing an effective ω-independent dielectric function which can be defined as

$$\frac{1}{\epsilon^{\text{eff}}} = 1 + F_c. \tag{A11}$$

Using the Penn dielectric function $\epsilon_{\text{Penn}}(q')$, we find that

$$\frac{1}{\epsilon^{\text{eff}}(q')} = \frac{1}{\epsilon_{\text{Penn}}(q')}\left[1 - \frac{E_g\sqrt{E_g^2+\omega_p^2+\beta^2 q'^2+(q'^4/4)}}{E_g^2+\beta^2 q'^2+(q'^4/4)}\right]\left[1 - \frac{E_g}{\sqrt{E_g^2+\omega_p^2+\beta^2 q'^2+(q'^4/4)}}\right]^{-1}. \tag{A12}$$

This equation shows that the static dielectric function $\epsilon_{\text{Penn}}(q')$ is corrected by the factor

$$F = \left[1 - \frac{E_g\sqrt{E_g^2+\omega_p^2+\beta^2 q'^2+(q'^4/4)}}{E_g^2+\beta^2 q'^2+(q'^4/4)}\right]\left[1 - \frac{E_g}{\sqrt{E_g^2+\omega_p^2+\beta^2 q'^2+(q'^4/4)}}\right]^{-1}. \tag{A13}$$

Instead of replacing $1/\epsilon(q')$ by (A12) to recalculate the optical absorption, we have chosen to calculate an average of F [Eq. (A13)] upon the q' space using Eq. (13) with the screened potential $V^{x,s}$ for the particular case $\tau_i = \tau_j = \tau_k = \tau_l = R_0 = 0$ (when $V^{x,s}$ takes its maximum value); this yields $\langle F \rangle = 0.87$.

In our approach, we assume that all the different $V^{x,s}$ terms appearing in the diagrams contributing to the dielectric function are reduced by that same factor of 0.87, due to those dynamical effects. This is the factor we have introduced above to incorporate those effects in the Penn's static dielectric function.

[1] W. Onida, L. Reining, and A. Rubio, Rev. Mod. Phys. **74**, 601 (2002).
[2] H. C. Weissker *et al.*, Phys. Rev. B **81**, 085104 (2010).
[3] L. Caramella, G. Onida, F. Finocchi, L. Reining, and F. Sottile, Phys. Rev. B **75**, 205405 (2007).
[4] I. Aguilera, J. Vidal, P. Wahnon, L. Reining, and S. Botti, Phys. Rev. B **84**, 085145 (2011).
[5] C. Noguez, J. Song, S. E. Ulloa, and D. A. Drabold, Superlatt. Microstruct. **20**, 405 (1996).
[6] X. Blase and P. Ordejon, Phys. Rev. B **69**, 085111 (2004).
[7] S. Brodersen, D. Lukas, and W. Schattke, Phys. Rev. B **66**, 085111 (2002).
[8] W. Hanke and L. J. Sham, Phys. Rev. B **12**, 4501 (1975).
[9] W. Hanke and L. J. Sham, Phys. Rev. B **21**, 4656 (1980).
[10] A. L. Fetter and J. D. Walecka, *Quantum Theory of Many-Particle Systems* (MacGraw-Hill, New York, 1971).
[11] J. P. Lewis, P. Jelinek, J. Ortega, A. A. Demkov, D. G. Trabada, B. Haycock, H. Wang, G. Adams, J. K. Tomfohr, E. Abad, H. Wang, and D. A. Drabold, Phys. Status Solidi B **248**, 1989 (2011); P. Jelinek, H. Wang, J. P. Lewis, O. F. Sankey, and J. Ortega, Phys. Rev. B **71**, 235101 (2005); J. P. Lewis, K. R. Glaesemann, G. A. Voth, J. Fritsch, A. A. Demkov, J. Ortega, and O. F. Sankey, *ibid.* **64**, 195103 (2001).
[12] M. S. Hybertsen and S. G. Louie, Phys. Rev. B **34**, 5390 (1986).
[13] S. G. Echenique, F. Flores, and R. H. Ritchie, *Dynamic Screening of Ions in Condensed Matter in Solid State Physics* (Academic, New York, 1990), Vol. 43.
[14] D. Pines, *Elementary Excitation in Solids* (Westview Press, Boulder, CO, 1999).
[15] M. A. Basanta, Y. J. Dappe, P. Jelínek, and J. Ortega, Comput. Mater. Sci. **39**, 759 (2007); O. F. Sankey and D. J. Niklewski, Phys. Rev. B **40**, 3979 (1989).
[16] D. J. Chadi and M. L. Cohen, Phys. Rev. B **8**, 5747 (1973).
[17] M. Fuchs and M. Scheffler, Comput. Phys. Commun. **119**, 67 (1999).
[18] W. Kohn and L. J. Sham, Phys. Rev. **140**, A1133 (1965).
[19] R. Stumpf and M. Scheffler, Comput. Phys. Commun. **79**, 447 (1994).
[20] P. Lautenschlager, M. Garriga, L. Vina, and M. Cardona. Phys. Rev. B **36**, 4821 (1987).
[21] *Semiconductors-Basic Data*, 2nd ed., edited by O. Madelung (Springer, Berlin, 1996).
[22] S. L. Adler, Phys. Rev. **126**, 413 (1962).
[23] N. Wiser, Phys. Rev. **129**, 62 (1963).
[24] F. Sottile, M. Marsili, V. Olevano, and L. Reining, Phys. Rev. B **76**, 161103(R) (2007).
[25] O. H. Crawford and C. W. Nestor, Phys. Rev. A **28**, 1260 (1983).
[26] J. M. Pitarke and I. Campillo, Nucl. Instrum. Methods Phys. Res., Sect. B **164**, 147 (2000).
[27] S. G. Louie, J. R. Chelikowsky, and M. L. Cohen, Phys. Rev. Lett. **34**, 155 (1975).
[28] M. Ehrnsperger and H. Bross, J. Phys.: Condens. Matter **9**, 1225 (1997).
[29] W. Schulke, J. R. Schmitz, H. Schulte-Schrepping, and A. Kaprolat, Phys. Rev. B **52**, 11721 (1995).
[30] J. F. Ziegler, *Hydrogen: Stopping Powers and Ranges in All Elements*, Vol. 3 of The Stopping and Ranges of Ions in Matter (Pergamon, Elmsford, New York, 1977).
[31] M. J. Berger, J. S. Coursey, M. A. Zucker, and J. Chang, Stopping-Power and Range Tables for Electrons, Protons, and Helium Ions http://physics.nist.gov/PhysRefData/Star/Text/PSTAR.html
[32] SRIM2013: Program SRIM2013, updated version of the J. F. Ziegler's, approximation [30]. http://www.srim.org/#SRIM
[33] I. Campillo, J. M. Pitarke, A. G. Eguiluz, and Alberto García, Nucl. Instrum. Methods Phys. Res., Sect. B **135**, 103 (1998).
[34] T. M. H. E. Tielens, G. E. W. Bauer, and T. H. Stoof, Phys. Rev. B **49**, 5741 (1994).
[35] W. M. Saslow and G. E. Reiter, Phys. Rev. B **7**, 2995 (1973).
[36] R. J. Mathar and M. Posselt, Phys. Rev. B **51**, 15798 (1995).